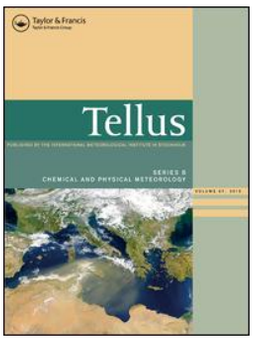

Tellus B: Chemical and Physical Meteorology

ISSN: (Print) 1600-0889 (Online) Journal homepage: http://www.tandfonline.com/loi/zelb20

State of mixing, shape factor, number size distribution, and hygroscopic growth of the Saharan anthropogenic and mineral dust aerosol at Tinfou, Morocco

N. Kaaden, A. Massling, A. Schladitz, T. MüLLER, K. Kandler, L. SchüTZ, B. Weinzierl, A. Petzold, M. Tesche, S. Leinert, C. Deutscher, M. Ebert, S. Weinbruch & A. Wiedensohler

To cite this article: N. Kaaden, A. Massling, A. Schladitz, T. MüLLER, K. Kandler, L. SchüTZ, B. Weinzierl, A. Petzold, M. Tesche, S. Leinert, C. Deutscher, M. Ebert, S. Weinbruch & A. Wiedensohler (2009) State of mixing, shape factor, number size distribution, and hygroscopic growth of the Saharan anthropogenic and mineral dust aerosol at Tinfou, Morocco, Tellus B: Chemical and Physical Meteorology, 61:1, 51-63, DOI: 10.1111/j.1600-0889.2008.00388.x

To link to this article: https://doi.org/10.1111/j.1600-0889.2008.00388.x

Published online: 18 Jan 2017.

Tellus
SERIES B
CHEMICAL
AND PHYSICAL
METEOROLOGY
PUBLISHED BY THE INTERNATIONAL METEOROLOGICAL INSTITUTE IN STOCKHOLM

Tellus (2009), 61B, 51–63
Printed in Singapore. All rights reserved

TELLUS

State of mixing, shape factor, number size distribution, and hygroscopic growth of the Saharan anthropogenic and mineral dust aerosol at Tinfou, Morocco

By N. KAADEN[1]*, A. MASSLING[1,2], A. SCHLADITZ[1], T. MÜLLER[1], K. KANDLER[3], L. SCHÜTZ[4], B. WEINZIERL[5], A. PETZOLD[5], M. TESCHE[1], S. LEINERT[6], C. DEUTSCHER[4], M. EBERT[3], S. WEINBRUCH[3] and A. WIEDENSOHLER[1], [1]*Leibniz Institute for Tropospheric Research, Leipzig, Germany;* [2]*Aarhus University, National Environmental Research Institute, Department of Atmospheric Environment, Roskilde, Denmark;* [3]*Institute for Applied Geosciences, Darmstadt University of Technology, Darmstadt, Germany;* [4]*Institute for Atmospheric Physics, Johannes-Gutenberg-University, Mainz, Germany;* [5]*Deutsches Zentrum für Luft- und Raumfahrt, Institut für Physik der Atmosphäre, Oberpfaffenhofen, 82234 Wessling, Germany;* [6]*Environmental Protection Agency, Richview, Dublin, Ireland*

(Manuscript received 6 February 2008; in final form 18 August 2008)

ABSTRACT

The Saharan Mineral Dust Experiment (SAMUM) was conducted in May and June 2006 in Tinfou, Morocco. A H-TDMA system and a H-DMA-APS system were used to obtain hygroscopic properties of mineral dust particles at 85% RH. Dynamic shape factors of 1.11, 1.19 and 1.25 were determined for the volume equivalent diameters 720, 840 and 960 nm, respectively.

During a dust event, the hydrophobic number fraction of 250 and 350 nm particles increased significantly from 30 and 65% to 53 and 75%, respectively, indicating that mineral dust particles can be as small as 200 nm in diameter. Log-normal functions for mineral dust number size distributions were obtained from total particle number size distributions and fractions of hydrophobic particles. The geometric mean diameter for Saharan dust particles was 715 nm during the dust event and 570 nm for the Saharan background aerosol.

Measurements of hygroscopic growth showed that the Saharan aerosol consists of an anthropogenic fraction (predominantly non natural sulphate and carbonaceous particles) and of mineral dust particles. Hygroscopic growth and hysteresis curve measurements of the 'more' hygroscopic particle fraction indicated ammonium sulphate as a main component of the anthropogenic aerosol. Particles larger than 720 nm in diameter were completely hydrophobic meaning that mineral dust particles are not hygroscopic.

1. Introduction

The Saharan desert is globally one of the major natural sources for mineral dust particles. The source strength varies between 130 and 5000 $Tg \cdot yr^{-1}$ (Swap et al., 1996; Cakmur et al., 2006; Goudi and Middleton, 2006). Dust plumes spreading from North Africa over the Atlantic Ocean are observed during the whole year (Moulin et al., 1997; Engelstaedter et al., 2006).

Maring et al. (2003) investigated particle number size distributions of Saharan dust in the outflow from the African continent at the Canary Islands and Puerto Rico. They found invariant particle number size distributions for both locations until a size of 7.3 μm. Only for larger diameters (>7.3 μm), a change in the distribution was observed as particles were removed most probably by sedimentation from the atmosphere during the transport over the Atlantic Ocean. However, up to now there is no data on particle number size distributions of Saharan aerosol in the source region obtained within the last 10 yr.

Particle number size distributions are crucial for determining aerosol radiative impacts (Tegen and Fung, 1994). Optical properties depend on the size and shape of the particles (Covert et al., 1972; Quinn et al., 1996; Tegen et al. 1996; Heintzenberg et al., 1997), which in turn vary due to hygroscopic growth. Especially for the understanding of remote sensing data, the knowledge of particle shape is of great interest in terms of their optical properties. Dubovic et al. (2002) showed that in comparison to Mie theory, a model simulating the irregularity of a particle improves the dust-particle phase function and size distribution.

*Corresponding author.
e-mail: kaaden@tropos.de
DOI: 10.1111/j.1600-0889.2008.00388.x

Mishchenko et al. (1997) also reported that the phase function is influenced by the particle shape and concluded that Mie theory cannot be used to calculate the phase function of dust particles.

Dust particles provide reactive sites for heterogeneous reactions with, for example, HNO_3 (Bauer et al., 2004). Acidification of mineral dust particles, for example, by nitric acid may lead to a significant uptake of water (Laskin et al., 2005) and thus to an increase in size and a change in shape. Levin et al. (1996) stated that desert dust particles larger than 1 μm in diameter are coated with sulphate and other soluble materials after contact with clouds (cloud processing). Since the particles were transported hundreds of kilometres, they are liable to lots of aging processes. There are speculations if dust particles in the source region already consist of a certain mass fraction of soluble material. However, there are no measurements about hygroscopic growth for Saharan dust particles in the source region. Hygroscopic properties of the Asian desert dust particles have been investigated in the outflow of China (Massling et al., 2007). No hygroscopic growth was observed there for the Asian dust particles.

Knowledge on the state of mixing of aerosol particles provides information on sources, transformation, and aging processes of the aerosol population. An important issue concerning the state of mixing was shown by Wang and Martin (2007), who discussed aerosol optical properties via satellite observations. They detected that the change from internal to external mixing for the insoluble and soluble materials changed the single scattering albedo, the aerosol optical depth, and the aerosol effective radius. For the interpretation of optical properties of ambient aerosols from satellite measurements, it is thus of great importance to know how the aerosol is mixed. Wang and Martin (2007) also comment that assumptions about the state of mixing in retrieval algorithms affect the deviated number concentration.

A comprehensive field study close to the Saharan desert was conducted to investigate and better understand the shape factor, number size distributions, state of mixing, and the hygroscopic growth of the Saharan aerosol for background and dusty conditions. During May and June, 2006, in situ ground-based measurements were performed as part of the Saharan Mineral Dust Experiment (SAMUM). Particle number size distributions have been measured directly in the size range from 20 nm up to 10 μm. Shape factors, state of mixing, size distributions of hydrophobic particles and hygroscopic growth of individual particle groups were derived from size-resolved hygroscopicity measurements in the size range from 30 nm up to 1 μm in dry diameter.

2. Methods

2.1. Location

For the SAMUM field experiment, a location close to the Saharan desert was chosen, which also provided a certain infrastructure for the measurement container. The 'Kasbah Hotel Porte au Sahara', a hotel near the small village Tinfou (30.14°N, 5.36°W; 684 m a.s.l.) 35 km southeast of Zagora in Southern Morocco was thus chosen as measurement site. The Saharan desert begins approximately 60 km south of Zagora.

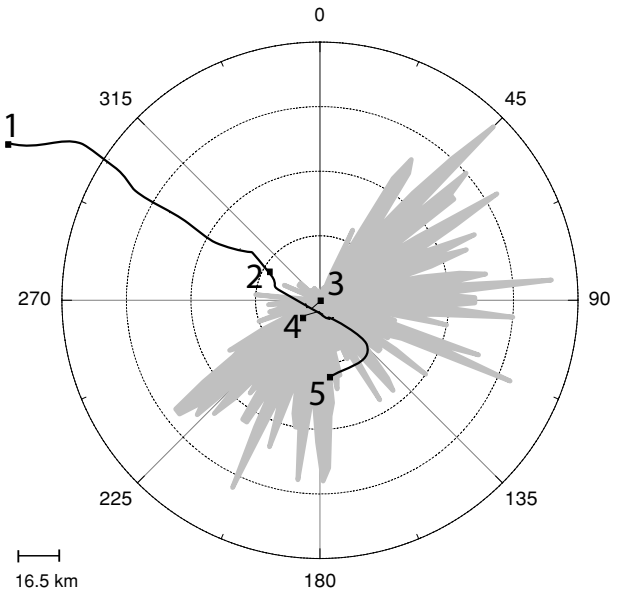

Fig. 1. Wind rose for the whole measuring period with the hotel (3) being situated in the center of the chart. The black line describes the road from Quarzazate (1) over Zagora (2) passing Tinfou (4) and ends in M'Hamid (5).

Two main wind directions prevailed during the field experiment which is shown as wind rose in Fig. 1. Next to the wind rose, the street from Quarzazate (1) with adjacent villages and the hotel (3) in the centre of the chart are shown. The container was located about 100 m northeast of the hotel. Since the hotel used mostly electrical power, contamination during the measurements occurred most probably only from the street. Data did undergo a quality check (e.g. peaks in number concentration), so that strong local contamination is excluded for the results shown here. A more detailed description of the measuring site is given in Heintzenberg (2008) and Kandler et al. (2008).

2.2. Instrumentation

All instruments were placed inside an air-conditioned sea container. To avoid strong heating inside the container, white awnings were placed around the container to reflect incoming solar radiation. An inlet system consisting of a low flow PM10 impactor was used to collect the ambient aerosol. Inside of the container, the aerosol was conducted to the individual instruments.

Two systems were applied, a Hygroscopicity-Tandem Differential Mobility Analyzer (H-TDMA; Massling et al., 2003) and a Hygroscopicity-Differential Mobility Analyzer-Aerodynamic

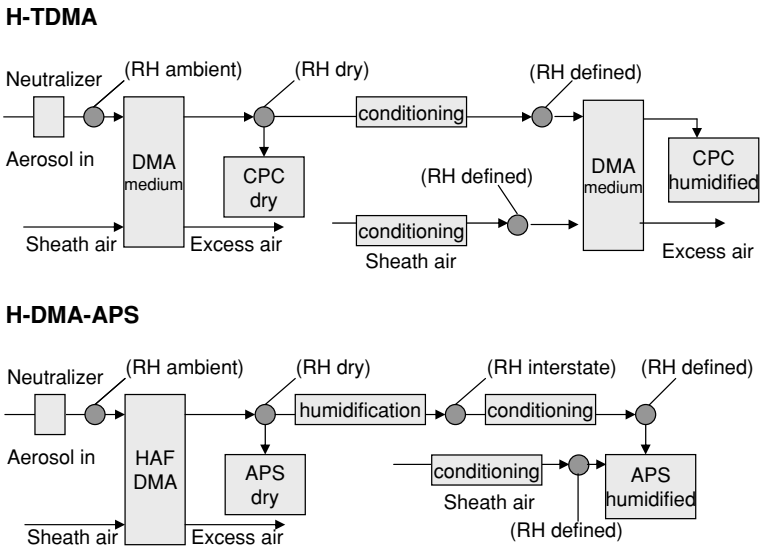

Fig. 2. Schematic set-up of the Hygroscopicity-Tandem Differential Mobility Analyzer (H-TDMA) and the Hygroscopicity-Differential Mobility Analyzer-Aerodynamic Particle Sizer (H-DMA-APS), the last one including a custom-made high aerosol flow-DMA (HAF-DMA).

Particle Sizer (H-DMA-APS; Leinert and Wiedensohler, 2008) to determine the state of mixing, shape factor, size distributions of hydrophobic particles, and hygroscopic growth of individual particle groups. These two systems work similarly with differences in the sampling technique and operating size range. Figure 2 illustrates a schematic set-up for both instruments.

The aerosol is dried by passing an aerosol diffusion dryer first and then charged in a custom-made Kr85 neutralizer to bring the particles into the bipolar charge equilibrium.

2.2.1. H-TDMA Quasi-monodisperse (certain electrical mobility) particle fractions (mobility diameters of 30, 50, 80, 150, 250 and 350 nm) are selected in the first Differential Mobility Analyzer (DMA; Knutson and Whitby, 1975; here: type Hauke medium). These quasi-monodisperse particles are divided into two parts afterwards. One part is conducted to a Condensation Particle Counter (CPC, TSI 3010, TSI Inc., St. Paul, MN, USA) that measures the number concentration of the selected dry particles. The second part is conditioned to a defined relative humidity (RH) by a humidity conditioner based on a Nafion membrane, in this case to 85%. The second DMA (again Type Hauke medium) together with the second CPC (again TSI 3010) is used as a mobility size spectrometer measuring the number size distribution of the humidified aerosol at 85% RH.

2.2.2. H-DMA-APS The H-DMA-APS is similar in function, but there are slight differences. The particles are selected in the mobility diameter range around 1 μm using a custom-made high aerosol flow—DMA (HAF-DMA) designed for an aerosol flow rate of 2 l min^{-1} and sheath air flow rate of 20 l min^{-1} (Leinert and Wiedensohler, 2008). Again, the quasi-monodisperse aerosol is divided into two parts downstream of the DMA. The first fraction of the aerosol is led to an Aerodynamic Particle Sizer (APS, TSI 3320, TSI Inc., St. Paul MN, USA) to determine the dry number size distribution (aerodynamic diameter) of the selected dry mobility diameters (here 800, 1000 and 1200 nm). The second aerosol fraction is conditioned by Nafion membranes to 85% RH. The number size distribution of the humidified aerosol is then obtained in a second APS operated with a sheath air flow humidified to 85%, too.

For both systems, regular calibration scans with ammonium sulphate were performed to recalculate the real humidity inside the second DMA (H-TDMA) and the second APS (H-DMA-APS). Furthermore, polystyrene latex (PSL) scans in the H-DMA-APS were taken to correct for size shifts of the APS instruments.

Next to the instruments for measuring the hygroscopicity, also a differential mobility particle sizer (DMPS; Birmili et al., 1999) in combination with an APS was applied. With these instruments, the particle number size distribution in the range from 20 nm up to 10 μm was obtained. Detailed information about the particle number size distribution can be found in Schladitz et al. (2008).

2.3. Calculations

Atmospheric aerosol particles are generally divided into groups of different hygroscopic growth depending on their origin and transformation history. From the H-TDMA and H-DMA-APS data, hygroscopic growth factors (gf) of different hygroscopic particle groups and their corresponding number fractions (nf) can be determined. Additionally, the dynamic shape factor (χ) can be determined from the H-DMA-APS measurements.

The hygroscopic growth factor is defined as the ratio of the humidified (wet) to the dry diameter of the same particle:

$$\mathrm{gf} = \frac{d_{\mathrm{ve,wet}}}{d_{\mathrm{ve,dry}}}, \tag{1}$$

with d_{ve} being the volume equivalent diameter. The individual systems use different diameter definitions for sizing. DMA

measurements are based on the mobility diameter (d_m), which can easily be converted into a volume equivalent diameter by knowledge of the particle shape factor (Hinds, 1999; DeCarlo et al., 2004). The APS measures an aerodynamic diameter (d_a). To calculate the volume equivalent diameter from d_a, the particle density (ρ_P) and the shape factor must be known. Both equations are described below, neglecting the Cunningham correction since it changes results in the third decimal place.

$$d_{ve} = \frac{d_m}{\chi}, \tag{2}$$

$$d_{ve} = d_a\sqrt{\chi . \frac{\rho_0}{\rho_P}}. \tag{3}$$

Hereby, ρ_0 is the unit density of 1.0 g cm^{-3}. The density of dry particles is obtained as material density from the electron-microscopic single particle analysis (Kandler et al., 2008). This material density and the effective density for aerodynamic processes are not necessarily equal, for example for agglomerates. Since agglomerates which influence the particle density are not the majority found in the samples it is stated, that the mineral density is realistic. Combining eqs (2) and (3) results in an equation for the dynamic shape factor:

$$\chi = \sqrt[3]{\frac{d_m^2}{d_a^2} . \frac{\rho_P}{\rho_0}}. \tag{4}$$

Since d_m is derived for dry particles, χ obtained by eq. (4) is only valid for dry particles.

With the H-TDMA, particles in the size range smaller than 350 nm are measured. Because the particles are relatively small, the shape of these particles can be assumed to be spherical. This assumption was confirmed by a study of Wu and Colbeck (1996). There, a linear relationship between the logarithm of d_{ve} and the logarithm of χ was found. This calculation was applied to the results obtained by the H-DMA-APS measurements showing that the dynamic shape factor reaches Unity at approximately 500 nm in volume equivalent diameter (see Section 3.1). Therefore, the mobility diameter for particles smaller than 500 nm equals the volume equivalent diameter and the growth factor can be calculated as shown in eq. (1).

The situation for the H-DMA-APS is more complicated. Calculation of the growth factor also follows eq. (1), but d_{ve} first has to be substituted with d_a for every single scan, leading to eq. (5):

$$gf = \frac{d_{ve,wet}}{d_{ve,dry}} = \frac{d_{a,wet}}{d_{a,dry}} . \sqrt{\frac{\chi_{wet} . \rho_{P,dry}}{\chi_{dry} . \rho_{P,wet}}} = gf_a . \sqrt{\frac{\chi_{wet} . \rho_{P,dry}}{\chi_{dry} . \rho_{P,wet}}}, \tag{5}$$

with gf_a being the aerodynamic growth factor.

Equation (5) includes two unknown parameters, the wet density ($\rho_{P,wet}$) and the wet shape factor (χ_{wet}). $\rho_{P,dry}$ and χ_{dry} are obtained as mentioned above. In the case that the particles do not grow by water uptake, $\rho_{P,wet}$ and χ_{wet} equal $\rho_{P,dry}$ and χ_{dry}, respectively. The growth factor is equal to the aerodynamic growth factor. In the case that the particles are strongly growing, χ_{wet} is Unity and $\rho_{P,wet}$ has to be assigned iteratively and converges to that of pure water at high RH. The iteration is done by the assumption that $\rho_{P,wet}$ is the ratio of the added masses (of the dry particle and the condensed material, which is in this case water) and the added volumes (of the dry particle and the condensed material). This assumption is included in eq. (5) resulting in eq. (6). For all other cases, both wet parameters have to be determined iteratively. Therefore, χ_{wet} has to be assigned under reasonable physical considerations. Here, a simple parameterization of χ_{wet} is used following the condition that in the growth factor range between 1.1 and 1.4, χ_{wet} converges from χ_{dry} to Unity in hyperbola form as expressed in eq. (7).

$$gf_a = \sqrt{\frac{\chi_{wet}}{\chi_{dry}} . \frac{1 + (gf^3 - 1)\frac{\rho_0}{\rho_{dry}}}{gf}}, \tag{6}$$

$$\chi_{wet} = \frac{\chi_{dry} - 1}{10} + 1 \,(\text{for} 1.1 < gf_a < 1.4). \tag{7}$$

Usually, more than one particle group in terms of hygroscopic growth is observed in particle number size distributions at high RH. Particles are usually separated into a 'more' hygroscopic, a 'less' hygroscopic and a hydrophobic particle group. Classification was done based on measured hygroscopic growth factors as follows: hydrophobic (gf < 1.15), 'less' hygroscopic (1.15 < gf < 1.45), and 'more' hygroscopic (gf > 1.4) particle fractions. The integral of the humidified particle number size distribution delivers the total number of particles N observed during the measurement. Thus, the particle number fraction of individual hygroscopic particle groups nf_i can be obtained by the ratio of number of particles of this individual group N_i and the total number of particles N_{tot}, following eq. (8):

$$nf_i = \frac{N_i}{N_{tot}}. \tag{8}$$

Uncertainties of the measured and calculated parameters were obtained by an error estimate and by propagation of errors, respectively. This leads to an error of approximately 4% for the hygroscopic growth factor for the H-TDMA after correction for the DMA shift and 14% for the number fraction. For the H-DMA-APS, the error for the growth factor is approximately 1.5%. There is an error of about 10% for the number fraction, although just one mode was found leading to a number fraction of 1. The error for the shape factor is approximately 15%, taking the uncertainty of the dry density of 15% into account.

2.4. *Instrumentation and methods of project partners*

Next to the results from hygroscopic measurements, results from other measurement techniques are compared. On board the 'Falcon' research aircraft of the DLR (Deutsches Zentrum für Luft- und Raumfahrt), extensive aerosol in situ instrumentation was operated (Weinzierl et al., 2008). Volatility

measurements were performed in the diameter range from 10 nm to 2.5 μm by a combination of particle sizing instruments with a thermal denuder (TD) (Clarke, 1991). The heating temperature of the TD was set to 250 °C in order to remove high to medium volatility organics, sulphuric acid and ammonium sulphate while leaving behind compounds with lower vapourization pressures like BC, sea salt, dust and crust material (Pinnick et al., 1987; Rose et al., 2006). More detail on the airborne volatility measurements performed during SAMUM is given in Weinzierl et al. (2008).

Other measurements were also performed at the airport of Quarzazate. The main focus at this location was remote sensing. One of the three lidars at Quarzazate airport was the IfT-six-wavelength Raman lidar Backscatter Extinction lidar-Ratio Temperature Humidity profiling apparatus (BERTHA; Althausen et al., 2000). With this lidar, laser pulses at 355, 400, 532, 710, 800 and 1064 nm wavelength are transmitted. The Raman lidar BERTHA was used to obtain profiles of the backscatter coefficient, the extinction coefficient, the extinction-to-backscatter ratio (lidar-ratio), and the depolarization ratio (Tesche et al., 2008).

At the hotel site near Tinfou, particle sampling was performed parallel to measurements with the H-TDMA and the H-DMA-APS. Analysis of these samples was amongst others conducted with electron-microscopic single particle analysis. With scanning electron microscopy (FEI ESEM 310 Quanta 200 FEG, Eindhoven, The Netherlands), several thousand particles were analyzed. The size of the particles is given in volume equivalent diameter (Kandler et al., 2008). The morphology and chemical composition of the particles was determined by energy-dispersive X-ray microanalysis. For smaller particles (<700 nm), this had to be done manually, since automatic analysis is not reliable.

2.5. Air mass classification

During the four week field study in May–June 2006, several changes in air mass derivation occurred. Different origins of the Saharan aerosol were identified based on meteorological time series and 2-d backward trajectories (Knippertz et al., 2008). Although some errors can occur regarding backward trajectories, the time frame of 2 d is small enough to get useful information about aerosol source and transport. Two representative periods have been selected for the whole time period to characterize different aerosol types during the experiment.

(1) *Saharan background*: This first classification describes the main streaming observed during the SAMUM field study. Two separated time periods, 16 to 19 May and 2 to 7 June 2006 were chosen to describe this air mass type. The air passed over Algeria and arrived in Tinfou from eastward direction. Sometimes, these air masses originated from the northeastern part of North Africa and crossed the Mediterranean Sea during advection to the measuring place. The wind velocity, recorded by an acoustic anemometer, reached a value of approximately 5 m s^{-1} and the visibility amounted to 10–30 km in average observed by a VPF-710 visibility sensor.

(2) *Mineral dust event*: One strong local dust event occurred from 22 to 26 May 2006. Backward trajectories did not show a distinct origin, but some trajectories arrived from southern directions and therewith from more central parts of the Saharan desert. The wind velocity reached a value of 16 m s^{-1} and the mean visibility was below 10 km.

3 Results and discussion

As mentioned above, all particle diameters presented here are converted from mobility or aerodynamic diameter to volume equivalent diameter. The reason for this conversion is that optical properties depend on the particle volume rather than on their mobility or aerodynamic properties.

To get a picture of the whole campaign data at a glance, wind speed and direction as well as number concentration for particles smaller than 100 nm and larger than 600 nm and the soot concentration are plotted in Fig. 3. In this figure, also the two representative periods are shown.

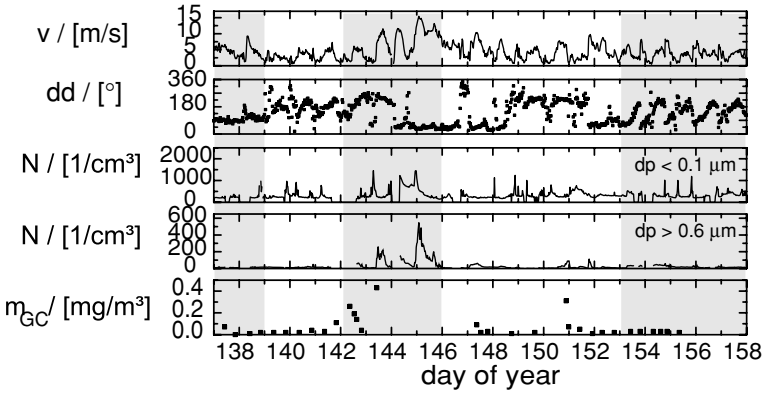

Fig. 3. Time series of wind speed (v) and wind direction (dd), number concentrations (N) of particles smaller than 100 nm and larger than 600 nm and soot mass concentrations (m_{GC}). The shaded areas present the different periods for the Saharan background (areas 1 and 3) and the dust event (area 2).

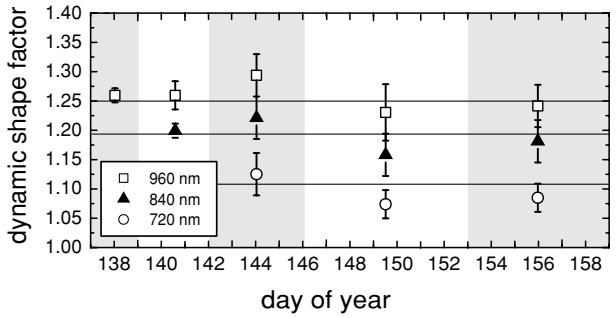

Fig. 4. Time series of mean values of the dynamic shape factor χ with standard deviation derived from the H-DMA-APS measurements. The black lines indicate the mean values for the whole period with 1.11, 1.19 and 1.25 for 720, 840 and 960 nm, respectively. The shaded areas present the different periods for the Saharan background (areas 1 and 3) and the dust event (area 2).

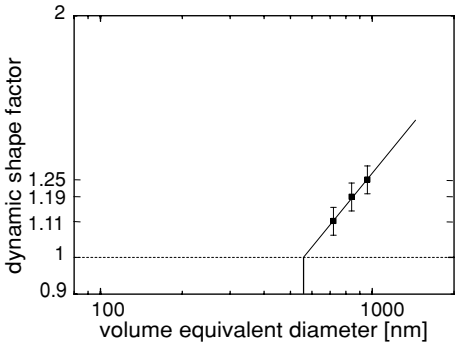

Fig. 5. Power law function of the dynamic shape factor for Saharan mineral dust particles as a function of the volume equivalent diameter. A shape factor of Unity is reached at a size of approximately 550 nm by extrapolating the linear function in the double logarithmic diagram.

3.1. Shape factor

There are different ways (by flow measurements or by microscopy) to obtain the shape factor of non-spherical particles (Davies, 1979). The shape factor obtained by flow measurements (here with the DMA and APS) is called dynamic shape factor and characterizes the three-dimensional particle. In contrast, shape factors obtained by microscopy are called aspect ratio (ratio of longest dimension to the orthogonal width) and are derived by a two-dimensional image.

The dynamical shape factor can be derived from the mobility and aerodynamic diameter of the particle if the particle density is known (eq. (4)). From electron-microscopic single particle analysis (Kandler et al., 2008), the particle density of mineral dust particles was determined to $\rho = 2.45$ g cm$^{-3} \pm 15\%$. This value is the volume-weighted average of the bulk densities of identified mineral phases for several thousands of individual particles. The H-DMA-APS measurements have been performed for mobility diameters of 800, 1000 and 1200 nm. Since for these mobility diameters also the aerodynamic size was measured with the APS operated at dry conditions, it was possible to calculate the dynamic shape factor for these dust particles according to eq. (4) using the particle density given above. Time series of the calculated dynamic shape factors are plotted in Fig. 4. Generally, the dynamic shape factor increases with increasing dry particle size. This result was also found by Reid et al. (2003) and Okada et al. (2001). The average dynamic shape factors for the above given mobility diameters range from 1.11 to 1.25 for the smallest to the largest mobility diameter, respectively. Using the above determined average shape factors, volume equivalent diameters of the H-DMA-APS measurements were retrieved from the mobility diameters. The corresponding volume equivalent diameters are 720, 840 and 960 nm, respectively. Davies (1979) gave a dynamic shape factor of 1.36 for quartz, which was determined for particles in the size range of 4–9 μm. Unfortunately no literature value for the dynamic shape factor of silicates was found, which was the main component for dust particles during the SAMUM field experiment.

Experimental data in the literature has shown that there is a power-law relationship between dynamic shape factor and volume equivalent diameter (Wu and Colbeck, 1996). Most of these literature data show an increase of the dynamic shape factor with increasing volume equivalent diameter. In Fig. 5, the dynamic shape factor is plotted as function of the volume equivalent diameter. A power law function is fitted through the shape factor values indicating that the dynamic shape factor of particles smaller than 500 nm is Unity. This result was also applied to adapt the number size distribution measurements from the DMPS and APS (Schladitz et al., 2008) for sizes larger than approximately 500 nm. The particle sizes of the H-TDMA measurements were thus not corrected for shape as also mentioned above.

Okada et al. (2001) reported about a median aspect ratio of 1.4 for desert dust particles in the size range of 500–1000 nm collected in arid regions of China. For the SAMUM experiment, in the similar size range (600–1000 nm), a median aspect ratio of 1.6 was observed except for gypsum with an aspect ratio of 1.71. Unfortunately, comparisons between aspect ratio and dynamic shape factor are not possible since the aspect ratio is independent of size (Okada et al., 2001). This size independence was also found for Saharan dust particles above 500 nm in diameter from electron-microscopic single particle analysis (Kandler et al., 2008).

3.2. State of mixing and number size distribution

The state of mixing provides information about the particle composition (internal and external mixing) as a function of particle size. In general, aerosol particles can be externally or internally mixed or they are a mixture of both. Using the results of the H-TDMA and H-DMA-APS measurements, the state of mixing

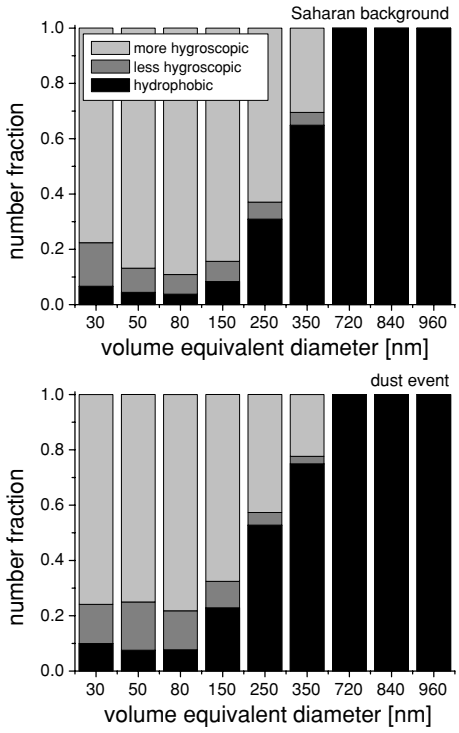

Fig. 6. Number fractions of the 'more' hygroscopic, 'less' hygroscopic, and hydrophobic particle groups measured with the H-TDMA and H-DMA-APS for the Saharan background aerosol and the mineral dust event.

of particles can be retrieved regarding the hygroscopic growth of individual particle groups of a certain particle size. These results also provide indications about the chemical composition of the observed particles.

In the case of H-TDMA measurements (30–350 nm), particles of one size grow differently at one selected relative humidity depending on the amount of soluble particle material, resulting in the above mentioned different particle groups. For the H-DMA-APS, just one particle group was observed. During the SAMUM experiment, a relative humidity of 85% was used to study hygroscopic growth for sub- and one-micrometer particles.

All H-TDMA diameters show the presence of hydrophobic and hygroscopic particles, while in the H-DMA-APS size range only hydrophobic particles were observed. In Fig. 6, the number fractions of the different hygroscopic particle groups are presented for the Saharan background aerosol and a mineral dust event. It is clearly visible that the fraction of hydrophobic particles increases with increasing size and reaches Unity for particles with 720, 840 and 960 nm in volume equivalent diameter. The number fraction of hydrophobic particles in the size range from 150 to 350 nm increased significantly during the dust event, while the fractions for 30, 50 and 80 nm particles did also double, but were still under 10%. The hydrophobic fraction of 150 nm particles was more than doubled from 8 to 23% during the mineral dust event. Müller et al. (2008) showed that soot is the main absorber in the fine mode during the SAMUM experiment with concentrations being short above detection limit (see also Fig. 3). Thus it is believed that there might be a mixture of carbonaceous particles and mineral dust in the size classes between 150 and 250 nm, which is confirmed by Kandler et al. (2008) who found dust components down to 100 nm. At 250 and 350 nm particle size, the hydrophobic number fraction exceeds 50 and 75%, respectively. The size range above 250 nm seems to be dominated by mineral dust particles, while carbonaceous particles might be responsible for observed hydrophobic particle number fractions in the size range smaller than 150 nm. The major particle fraction (80–90%) of the 30–150 nm particles, however, is hygroscopic. These particles consist probably of a mixture of soluble and insoluble material. In contrast, the number fraction of hygroscopic particles for 250 and 350 nm decreases during the dust event. Nevertheless, hygroscopic particles form an omnipresent background close to the Saharan desert as well as soot does.

The same conclusion was drawn from volatility measurements in the range from 10 nm to 2.5 μm (aerosol was heated to 250 °C) taken on board the 'Falcon' over Zagora (Weinzierl et al., 2008). They found two different aerosol regimes, one below and one above 500 nm. The distinction of these different aerosols is described as externally mixed particles (<500 nm) and internally mixed particles (>500 nm). The state of mixing indicates different origins of the particles in these size ranges. The volatility measurements presented in Fig. 7 show the shrinking factor (sf) versus the volume equivalent diameter. The sf explains the value, to which the particles are shrinking due to volatilisation. A sf smaller than 0.5 was observed for particles up to 200 nm. This finding indicates that these particles consist mainly of volatile compounds such as sulphate. Between 150 and 300 nm, the sf suddenly increases from 0.5 to 0.8,

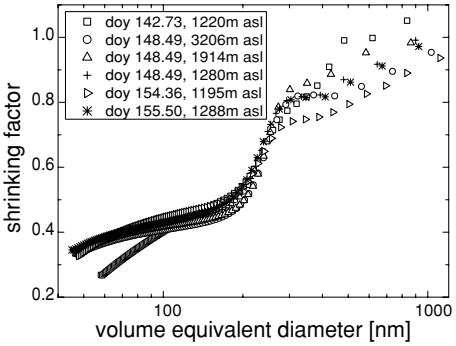

Fig. 7. Shrinking factor obtained by volatility measurements performed onboard the aeroplane 'Falcon' (Weinzierl et al., 2008) indicating shrinking of particles at 250°C. The flights of the 'Falcon' over Zagora were performed at different days and different flight levels as shown in the box inside the figure.

Table 1. Corresponding particle classes from electron-microscopic single particle analysis to groups of hygroscopic growth

Groups of hygr. growth	Particle class
'More' hygroscopic	Sodium chloride, sulphates, Ammonium sulphate
'Less' hygroscopic	Sulphate silicate mixtures, Others, other calcium rich
Hydrophobic	Iron-rich, titanium-rich, quartz, Calcium carbonates, gypsum, Carbonaceous, silicates

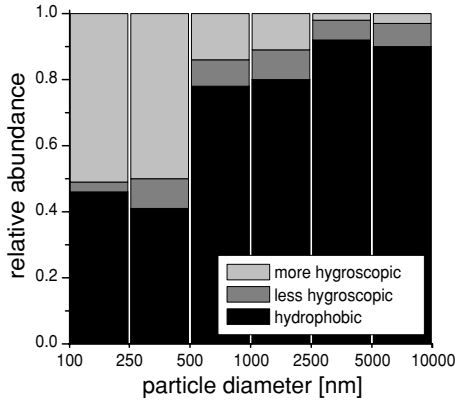

Fig. 8. Relative abundance of the different hygroscopic particle groups for different size intervals determined from single particle analysis (Kandler et al., 2008). Data show averages for several samples from May 13 to May 30, 2006.

indicating that a change in aerosol composition occurred. This observation agrees well with results from hygroscopicity measurements indicating a change in the dominating number fraction from hygroscopic to hydrophobic aerosol. For larger particles (>500 nm), the sf converges to the value of Unity (no shrinking) indicating non-volatile compounds such as mineral dust being the main compound.

The hygroscopic growth measurements could not provide data for the size range between 350 and 720 nm in volume equivalent diameter. Results from electron-microscopic single particle analysis can provide insight into the state of mixing for this size range. The relative abundance of different particle classes in terms of chemical composition (e.g. silicates and quartz) is combined with the grouping in terms of hygroscopic growth (Table 1). The abundance for the different hygroscopic groups averaged for certain days from May 13 to May 30 is shown in Fig. 8. A significant change is seen for particles larger than 500 nm in diameter as indicated before from the hygroscopicity and volatility measurements. At 500 nm particle size, dominating more hygroscopic components (relative abundance of sulphate is 55%) turn to dominating hydrophobic ones (mineral dust 80%). There is 15% of more hygroscopic material left. With the H-DMA-APS, a material abundance of at least 10% has to be present to 'see' this particle fraction in the measurements. By expecting that electron-microscopic single particle analysis also holds some errors, the possibility of a material abundance smaller than 10% is given. This can explain the differences for more hygroscopic particles larger than 500 nm in volume equivalent diameter between electron-microscopic single particle analysis (small fraction of hygroscopic particles) and the H-DMA-APS measurements (no hygroscopic particles).

A sudden increase of hydrophobic material was also observed in this size range by Iwasaka et al. (2003) reporting about measurements over the Asian continent. Since different compounds were found for the mineral dust aerosol, the state of mixing of one-micrometer particles may thus be internal with exclusively hydrophobic components.

The origin of the 'less' hygroscopic particle group for both periods may lay in the mixing or coating of hydrophobic with soluble material. Electron-microscopic single particle analysis showed a maximum for dust-sulphate mixtures between 250 and 500 nm of 6%. For the size range between 500 and 1000 nm, this value decreased to 2%. This shows that dust and ammonium sulphate particles are internally mixed but more commonly they are externally mixed.

In general, aerosol particles smaller than 150 nm in diameter probably represent a dust-independent anthropogenic background aerosol, which was also investigated by Müller et al. (2008), while particles larger than 250 nm consist mainly of mineral dust. In Fig. 9, average number size distributions of the Saharan background aerosol and the mineral dust event are plotted. The black dots represent the entire particle number size distribution, while the open stars indicate the fraction of hydrophobic particles. Log-normal size distributions were fitted for the mineral dust and the carbonaceous modes. The number peak of the hydrophobic carbonaceous particles is always approximately 110 nm, which is common for combustion aerosols. The geometric mean diameter of the mineral dust mode increases during dust events (715 nm) compared to background conditions (570 nm). This fact is not surprising since larger dust particles are lost by sedimentation during transport reducing the number concentration in the super-micrometer size range. The number concentration during mineral dust events is approximately five times higher than during background conditions. The geometric standard deviations lie in the range of 1.7–1.9.

3.3. Hygroscopic growth

As explained above, aerosol particles of a certain size can be divided into groups representing different hygroscopic growth behaviour und have thus different hygroscopic growth factors at high relative humidities above 80%.

As discussed before, the aerosol over the Saharan desert is divided into two independent mixed particle fractions. Internally mixed Saharan mineral dust particles dominate the

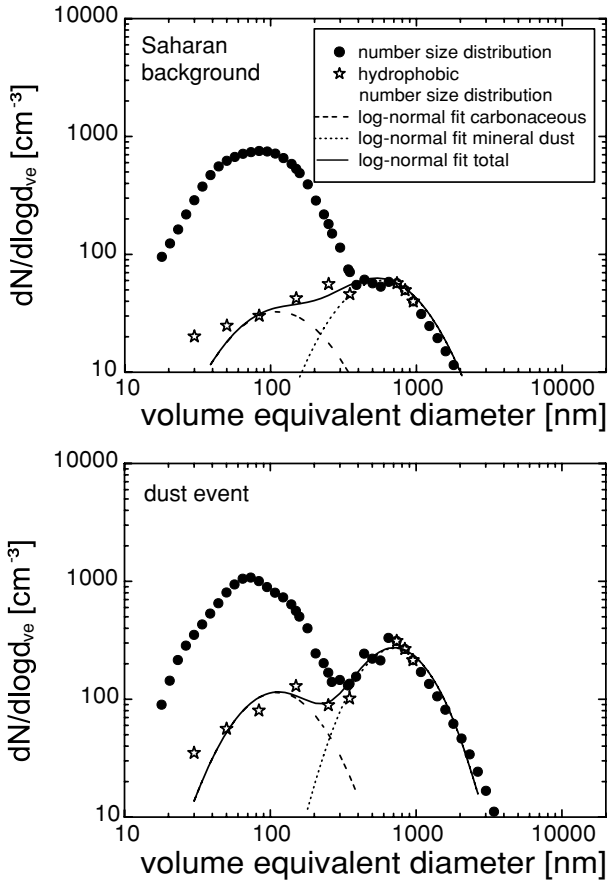

Fig. 9. Particle number size distribution for Saharan background aerosol and a mineral dust event. The number size distribution of hydrophobic particles is indicated by the stars and was fitted with log-normal functions resulting in a carbonaceous and a mineral dust mode.

size range above 250 nm, while externally mixed smaller particles are mainly of anthropogenic origin.

3.3.1. Mineral dust Hygroscopic properties of mineral dust particles have been determined using the H-DMA-APS and the H-TDMA systems. In Fig. 10, averaged hygroscopic growth factors are shown for different particle sizes for the Saharan background as well as for the Saharan dust event. Only hydrophobic particles have been found for the size range measured with the H-DMA-APS system. This finding has been independent of air mass and an instrumental error can be excluded since regularly salt scans showed particle growth. As discussed in the previous section, mineral dust particles can be as small as approximately 200 nm in diameter. The H-TDMA measurements show that during Saharan mineral dust events, the hydrophobic number fraction of 250 and 350 nm particles, which was always present, increased. The results of both systems indicate that mineral dust particles do not show a significant hygroscopic growth when observed close to their source.

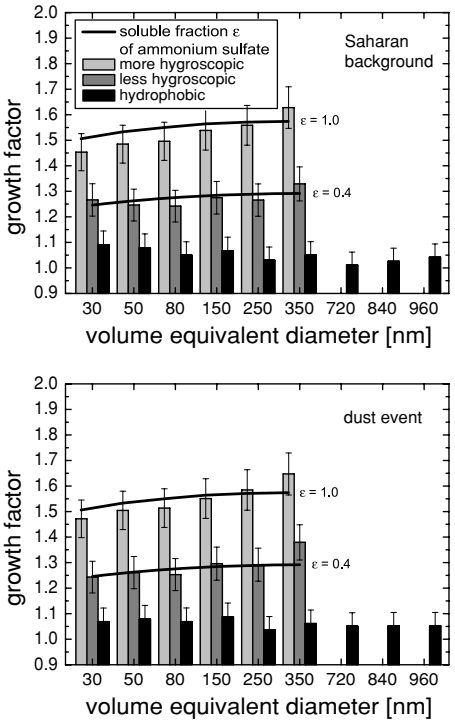

Fig. 10. Number fractions of the different hygroscopic particle groups for the Saharan background aerosol and the mineral dust event. The theoretical hygroscopic growth of ammonium sulfate is plotted as black line for soluble volume fractions of 1 and 0.4.

The non-uptake of water by mineral dust particles under ambient conditions is supported by lidar measurements performed at the airport of Ouarzazate, Morocco, within the field experiment SAMUM. Lidar measurements were accompanied by radiosonde soundings to derive profiles of meteorological parameters as well. The backscatter coefficient measured with lidar is mainly dominated by particles larger than one micrometer in diameter. Thus, the results predominantly show properties of large Saharan mineral dust particles. Figure 11 shows the backscatter

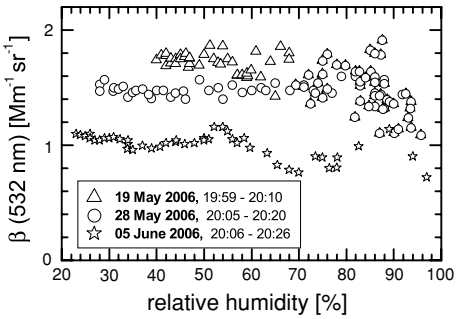

Fig. 11. Backscatter coefficient β at a wavelength of 532 nm measured with BERTHA as a function of relative humidity determined from radiosondes. No change in backscattering due to potential hygroscopic growth of mineral dust particles was observed at ambient conditions ranging from 20 to about 98% RH.

coefficient as a function of the relative humidity for May 19, May 28 and June 5, 2006. The days selected to present aerosol data are characterised by a high ambient RH (>80%) rather than the air mass types given above, in order to examine the hygroscopic behaviour in the vertical direction to compare with results obtained at ground level. Lidar profiles (Raman solution at 532 nm, 60 m smoothing length) were averaged over the time range that the radiosonde needed to reach the top of the dust layer. Thus, 10–20 min of lidar measurements were averaged depending on the depth of the dust layer and the ascend rate of the radiosonde. With increasing relative humidity no increase in the values of the backscatter coefficient was observed. In case of any water-uptake, lidar-derived properties would change instantly. Therefore it can be stated that no change of the backscatter coefficient due to potential hygroscopic growth of mineral dust particles was observed at ambient conditions, even if relative humidity was reaching values close to water vapour saturation at the top of the dust layer.

3.3.2. Anthropogenic aerosol The Saharan aerosol seems to carry anthropogenic particles for background conditions and during mineral dust events. This was already observed by Raes et al. (1997) at the Canary Islands in the free troposphere. The particle number size distributions show increased number concentrations of such particles in the size range below 200 nm. H-TDMA measurements show groups of particles with different hygroscopic growth for this size range. As shown in Fig. 10, hydrophobic particles are present for all sizes below 150 nm independent of the existence of mineral dust. These particles consist probably of carbonaceous compounds as mentioned above. A fraction of 10–15% of particles in the size range smaller 150 nm is 'less' hygroscopic meaning that hydrophobic particles are containing soluble material. Their growth factors range from 1.25 to 1.35 for particles with sizes between 30 and 350 nm.

The fraction of 'more' hygroscopic particles is largest for particle sizes smaller 150 nm and is always greater than 70% in these size classes. The 'more' hygroscopic particles show hygroscopic growth factors from 1.45 to 1.65 measured at 85% RH. For a better understanding of the chemical speciation of the observed particles, a simple two component solubility model (Swietlicki et al., 1999) was used calculating the volume fraction of soluble and insoluble compounds in the particle. Ammonium sulphate was used as input parameter for the solubility model to simulate the size-dependent hygroscopic growth factors by varying the soluble volume fraction (ε). The results imply that particles in the 'more' hygroscopic group grow nearly as pure ammonium sulphate (ε is nearly 1, so that nearly 100% of the particles consisted of ammonium sulphate). Particles in the 'less' hygroscopic group have a soluble volume fraction of approximately 0.4. These particles are internally mixed consisting of 40% soluble material, assuming ammonium sulphate as the major soluble compound.

Further measurements were done to prove if these hygroscopic particles were predominantly composed of ammonium sulphate or, for example, sulphuric acid. A pure inorganic salt particle (e.g. ammonium sulphate particle) shows a hysteresis behaviour in terms of its hygroscopic growth factor in dependence of RH, while a pure inorganic acid particle (e.g. sulphuric acid particle) continuously grows with increasing relative humidity (RH). Furthermore, the rapid increase of the growth factor at the deliquescence relative humidity (DRH) provides information about the type of salt observed.

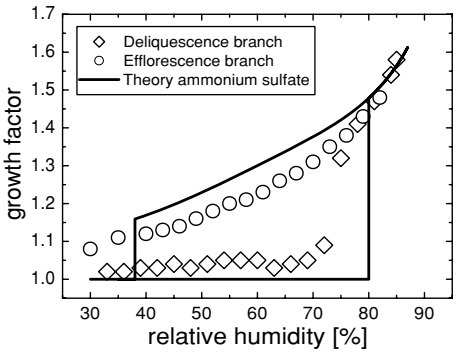

Fig. 12. Hysteresis behavior of initially dry 'more' hygroscopic 150 nm particles. Theoretical hysteresis curve for ammonium sulfate is plotted as black line.

The hysteresis measurements were performed for 150 nm dry particles on 5 June 2006 (Saharan background). The RH of the sheath air of the H-TDMA was stepwise increased for different values between 30 and 85%. The aerosol RH was increased the same way. After the sheath air reached 85% RH, it was stepwise decreased again, while the aerosol RH was held at 85% to ascertain that the aerosol particles were dried from a wet state. Results from this experiment are plotted in Fig. 12. The 'more' hygroscopic 150 nm particles show a clear hysteresis behaviour indicating an inorganic salt or a mixture of inorganic salts as dominating compound. The DRH of the observed particles was found at about 74.6% close to that of pure ammonium sulphate (79.6%) (Onasch et al., 1999), pure sodium nitrate (74.5%) (Tang and Munkelwitz, 1994) and pure sodium chloride (75.3%) (Tang and Munkelwitz, 1993) measured at 25 °C, respectively. Except for ammonium sulphate, the other salts can be excluded since they are unlikely to exist at 150 nm as major compound for this aerosol type. Furthermore, their theoretical growth factors do not fit with the measured values and they also were not found by single particle chemical analysis. The hysteresis curve of ammonium sulphate, based on parameterizations of Tang and Munkelwitz (1994), is plotted as black line in Fig. 12. Measured growth factors of the metastable branch (supersaturated solution) lie, however, beneath the theoretical values of pure ammonium sulphate and a recristallization point (RP) was not observed in the measurements. A possible explanation for the lower deliquescence point and the smaller hygroscopic growth factors is that the ambient particles were not composed of ammonium sulphate only. They may have been a mixture of different

compounds which are in turn in thermodynamic equilibrium with the gas phase [e.g. NH_3, $(NH_4)HSO_4$, H_2SO_4] at atmospheric conditions (Brosset, 1983) with ammonium sulphate being the dominating compound.

4. Conclusion

In situ ground-based measurements were performed in Tinfou, Morocco, to obtain physical properties of the Saharan aerosol for background conditions and during mineral dust events.

Shape factors of mineral dust, state of mixing, number size distribution of hydrophobic particles and hygroscopic growth have been determined using instrumentation operating in the sub- and one-micrometer size range to measure hygroscopic growth at a high relative humidity. Therefore, the H-TDMA and the H-DMA-APS systems were used to distinguish between hygroscopic and hydrophobic particles for certain mobility diameters (H-TDMA: $d_m = 30$, 50, 80, 150, 250 and 350 nm; H-DMA-APS: $d_m = 800$, 1000, 1200 nm).

From electron-microscopic single particle analysis, the density of particles around 1 μm in diameter was obtained to 2.45 g cm^{-3} $\pm$ 15%. Knowing this value, we were able to calculate the shape factors and the volume equivalent diameters for these particles from the mobility and aerodynamic diameter of the H-DMA-APS system. The shape factors are 1.11, 1.19 and 1.25 for the volume equivalent diameters 720, 840 and 960 nm, respectively resulting from the above given mobility diameters. The shape factors follow a power law as described in literature for non-spherical particles.

Fractions of hydrophobic particles were determined from the H-TDMA and H-DMA-APS. The results show that mineral dust particles are always (Saharan background and dust event) completely hydrophobic in the H-DMA-APS size range. This result implies no influence of potential emissions from dry salt lakes on the observed particle population at Tinfou, Morocco.

On the other hand, the H-TDMA measurements showed independent fractions of hydrophobic particles below 150 nm in diameter for background conditions and during mineral dust events. These particles are probably of carbonaceous nature. In the size range between 250 and 350 nm, the fraction of hydrophobic particles depends, however, on the occurrence of dust events. During those events, the number fraction of hydrophobic particles increases significantly indicating that mineral dust particles can be as small as 200 nm in diameter.

By combining the number fractions of hydrophobic particles and the measured number size distributions (corrected to volume equivalent diameter) we determined log-normal functions of the mineral dust and the carbonaceous aerosol. Mineral dust concentrations during dust events are approximately a factor of five higher than under Saharan background conditions. The geometric mean diameter for background conditions is 570 nm and increases during the dust event to 715 nm. The reason for the smaller mean diameter during background conditions are losses of larger particles during transport due to sedimentation. The geometric mean diameter of the carbonaceous particles is about 110 nm, which is typical for anthropogenically emitted combustion aerosols.

'More' and 'less' hygroscopic particles have only been found in the size range below 350 nm in diameter. The fraction of 'more' hygroscopic particles for particles smaller than 150 nm in diameter is always greater than 70%, while 'less' hygroscopic particles contribute by 10–15%. Using a simple two-component solubility model, the measured hygroscopic growth at 85% RH can be explained assuming 100% ammonium sulphate for the 'more' hygroscopic particles. The 'less' hygroscopic particles would then consist of 40% ammonium sulphate assuming 60% of the volume to be non soluble.

The hysteresis behaviour of 150 nm 'more' hygroscopic particles was measured in a single experiment. The deliquescence relative humidity was measured to 74.6%, 5% lower than that of pure ammonium sulphate. Additionally, the hygroscopic growth at the upper branch of the hysteresis below 70% relative humidity was slightly lower than that based on theoretical considerations. These results indicate that the composition of the hygroscopic particles mainly contains an ammonium and sulphate mixture, with ammonium sulphate being one of the major compounds of other ammonium and sulphate containing compounds, which may be in equilibrium in the atmosphere.

Conclusively, the Saharan aerosol consists of a combination of anthropogenic compounds and mineral dust. The anthropogenic component seems to exist continuously as a kind of background aerosol dominating the accumulation mode range up to 200 nm in diameter representing an externally mixed aerosol of ammonium sulphate/other inorganic components and carbonaceous particles. The second component is the Saharan mineral dust, which is also always present in different size regimes with varying number concentrations depending on meteorological conditions.

5. Acknowledgments

This study was supported by the German Research Foundation (DFG contract FOR 539) in the framework of the research group SAMUM.

References

Althausen, D., Müller, D., Ansmann, A., Wandinger, U., Hube, H. and co-authors. 2000. Scanning 6-wavelength 11-channel aerosol lidar. *J. Atmos Oceanic Technol.* **17**, 1469–1482.

Bauer, S. E., Balkanski, Y., Schulz, M., Hauglustaine, D.A. and Dentener, F. 2004. Global modeling of heterogeneous chemistry on mineral aerosol surfaces: Influence on tropospheric ozone chemistry and comparison to observations. *J. Geophys. Res.* **109**, doi: 10.1029/2003JD003868.

Birmili, W., Stratmann, F. and Wiedensohler, A. 1999. Design of a DMA-based size spectrometer for a large particle size range and stable operation. *J. Aerosol Sci.* **30**, 549–553.

Brosset, C. 1983. Characterization of acidity in natural waters. In: *Acid Deposition*. D. Reidel Publishing Co., Boston, pp. 44–55.

Cakmur, R.V., Miller, R.L., Perlwitz, J., Geogdzhayev, I.V., Ginoux, P., and co-authors. 2006. Constraining the magnitude of the global dust cycle by minimizing the difference between a model and observations. *J. Geophys. Res.* **111**, 1–24.

Clarke, A.D. 1991. A thermo-optic technique for in situ analysis of size-resolved aerosol physicochemistry. *Atmos. Environ.* **25A**, 635–644.

Covert, D., Charlson, R. and Ahlquist, N. 1972. A study of the relationship of chemical composition and humidity to light scattering by aerosols. *J. Appl. Meteorol.* **11**, 968–976.

Davies, C. N. 1979. Particle-fluid interaction. *J. Aerosol. Sci.* **10**, 477–513.

DeCarlo, P., Slowik, J., Worsnop, D. R. and Davidovits, P. J. J. 2004. Particle morphology and density characterization by combined mobility and aerodynamic diameter measurements. Part 1: theory. *Aerosol. Sci. Technol.* **38**, 1185–1205.

Dubovik, O., Lapyonok, T., Sinyuk, A., Mishchenko, M. I., Yang, P. and co-authors. 2002. Non-spherical aerosol retrieval method employing light scattering by spheroids. *Geophys. Res. Lett.* **10**, 54.1–54.4.

Engelstaedter, S., Tegen, I. and Washington, R. 2006. North African dust emission and transport. *Earth Sci. Rev.* **79**, 73–100.

Goudie, A. S. and Middleton, N. J. 2006. *Desert Dust in the Global System.* Springer, Heidelberg.

Heintzenberg, J., Charlson, R., Clarke, A., Liousse, C., Ramaswamy, V. and co-authors. 1997. Measurements and modelling of aerosol single scattering albedo: Progress, problems and prospects. *Beitr. Phys. Atmos*. **70**, 249–263.

Heintzenberg, J. 2008. The SAMUM–1 experiment over Southern Morocco: overview and introduction. *Tellus* **61B**, doi: 10.1111/j.1600-0889.2008.00403.x.

Hinds, W. C. 1999. *Aerosol Technology: Properties, Behaviour, and Measurement of airborne particles*. John Wiley & Sons. New York.

Iwasaka, Y., Shi, G.-Y., Yamada, M., Matsuki, A., Trochkine, D. and co-authors. 2003. Importance of dust particles in the free troposphere over the Taklamakan Desert: Electron microscopic experiments of particles collected with a balloonborne particle impactor at Dunhuang, China. *J. Geophys. Res.* **108**, 12.9–12.10.

Kandler, K., Schütz L., Deutscher C., Hofmann H., Jäckel S. and co-authors. 2008. Size distribution, mass concentration, chemical and mineralogical composition, and derived optical parameters of the boundary layer aerosol at Tinfou, Morocco, during SAMUM 2006. *Tellus* **61B**, doi: 10.1111/j.1600-0889.2008.00385.x.

Knippertz, P., Ansmann, A., Althausen, D., Müller, D., Tesche, M. and co-authors. 2008. Dust mobilization and transport in the Northern Sahara during SAMUM 2006—a meteorological overview. *Tellus* **61B**, doi: 10.1111/j.1600-0889.2008.00380.x.

Knutson, E. O. and Whitby, K. T. 1975. Aerosol classification by electric mobility: apparatus, theory and applications. *J. Aerosol Sci.* **6**, 443–451.

Laskin, A., Wietsma, T. W., Krueger, B. J. and Grassian, V. H. 2005. Heterogeneous chemistry of individual mineral dust particles with nitric acid: a combined CCSEM/EDX, ESEM, and ICP-MS study. *J. Geophys. Res*. **110**, 1–15.

Leinert, S. and Wiedensohler, A. 2008. A DMA and APS based technique for measuring aerodynamic hygroscopic growth factors of micrometer-size aerosol particles. *J. Aerosol Sci.* **39**, 393–402.

Levin, Z., Ganor, E. and Gladstein, V. 1996. The effects of desert particles coated with sulfate on rain formation in the eastern Mediterranean. *J. Appl. Meteorol.* **35**, 1511–1523.

Maring H., Savoie, D. L., Izaguirre, M. A. and Custal, L. 2003. Mineral dust aerosol size distribution change during atmospheric transport. *J. Geophys. Res.* **108**, 8.1–8.6.

Massling, A., Wiedensohler, A., Busch, B., Neus, C., Qiunn, P. and co-authors. 2003. Hygroscopic properties of different aerosol types over the Atlantic and Indian Ocean. *Atmos. Chem. Phys*. **3**, 1377–1397.

Massling, A., Leinert, S., Wiedensohler, A. and Covert, D. 2007. Hygroscopic growth of sub-micrometer and onemicrometer aerosol particles measured during Ace-Asia. *Atmos. Chem. Phys.* **7**, 3249–3259.

Mishchenko, M. I., Travis, L. D., Kahn, R. A. and West, R. A. 1997. Modeling phase functions for dust like tropospheric aerosol using a shape mixture of randomly oriented polydisperse spheroids. *J. Geophys. Res.* **102**, 16831–16847.

Moulin, C., Lambert, C., Dulac, F. and Dayan, U. 1997. Control of atmospheric export of dust from north Africa by the north Atlantic oscillation. *Nature*. **387**, 691–694.

Müller, T., Schladitz, A., Maßling, A., Kaaden, N. and Wiedensohler A. 2008. Spectral absorption coefficients and imaginary parts of refractive indices of Saharan dust during SAMUM-1. *Tellus* **61B**, doi: 10.1111/j.1600-0889.2008.00399.x.

Okada, K., Heintzenberg, J., Kai, K. and Qin, Y. 2001. Shape of atmospheric mineral particles collected in three Chinese arid-regions. *J. Geophys. Res.* **28**, 3123–3126.

Onasch, T. B., Siefert, T. L., Brooks, S. D., Prenni, A. J., Murray, B. and co-authors. 1999. Infrared spectroscopic study of the deliquescence and efflorescence of ammonium sulfate aerosol as a function of temperature. *J. Geophys. Res.* **104**, 21317–21326.

Pinnick, R. G., Jennings, S. G. and Fernandez, G. 1987. Volatility of aerosols in the arid southwestern United States. *J. Atmos. Sci.* **44**, 562–576.

Quinn, P., Anderson, T., Bates, T., Dlugi, R., Heintzenberg, J. and co-authors. 1996. Closure in tropospheric aerosol-climate research: a review and future needs for addressing aerosol direct shortwave radiation forcing. *Beitr. Phys. Atmos*. **69**, 547–577.

Raes, F., Van Dingenen, R., Cuevas, E., Van Velthoven. P. F. J. and Prospero, J. M. 1997. Observations of aerosols in the free troposphere and marine boundary layer of the subtropical Northeast Atlantic: discussion of processes determining their size distribution. *J. Geophys. Res.* **102**, 21315–21328.

Reid, E. A., Reid, J. S., Meier, M. M., Dunlap, M. R., Cliff, S. S. and co-authors. 2003. Characterization of African dust transported to Puerto Rico by individual particle and size segregated bulk analysis. *J. Geophys. Res.* **108**, 7.1–7.22.

Rose, D., Wehner, B., Ketzel, M., Engler, C.,Voigtländer, J. and co-authors. 2006. Atmospheric number size distributions of soot particles and estimation of emission factors. *Atmos. Chem. Phys.* **6**, 1021–1031.

Schladitz, A., Müller, T., Massling, A., Kaaden, N., Kandler, K. and co-authors. 2008. In situ measurements of Optical Properties at Tinfou (Morocco) during the Saharan Mineral Dust Experiment SAMUM 2006. *Tellus* **61B**, doi: 10.1111/j.1600-0889.2008.00397.x.

Swap, R., Ulanski, S., Cobett, M. and Garstang, M. 1996. Temporal and spatial characteristics of Saharan dust outbreaks. *J. Geophys. Res.* **101**, 4205–4220.

Swietlicki, E., Zhou, J., Berg, O., Martinsson, B., Frank, G. and co-authors. 1999. A closure study of sub-micrometer aerosol particle hygroscopic behaviour. *Atmos. Res.* **50**, 205–240.

Tang, I. N. and Munkelwitz, H. R. 1993. Composition and temperature dependence of the deliquescence properties of hygroscopic aerosols. *Atmos. Environ.* **27A**, 467–473.

Tang, I. and Munkelwitz, H. 1994. Water activities, densities, and refractive indices of aqueous sulfates and sodium nitrate droplets of atmospheric importance. *J. Geophys. Res.* **99**, 18801–18808.

Tegen, I. and Fung, I. 1994. Modeling of mineral dust in the atmosphere' sources, transport, and optical thickness. *J. Geophys. Res.* **99**, 22 897–22 914.

Tegen, I., Lacis, A. and Fung, I. 1996. The influence on climate forcing of mineral aerosols from disturbed soils. *Nature*. **380**, 419–422.

Tesche, M., Ansmann, A., Müller, D., Althausen, D., Mattis, I. and co-authors. 2008. Vertical profiling of Saharan dust with Raman lidars and airborne HSRL in southern Morocco during SAMUM. *Tellus* **61B**, doi: 10.1111/j.1600-0889.2008.00390.x.

Wang, J. and Martin, S. 2007. Satellite characterization of urban aerosols: importance of including hygroscopicity and mixing state in the retrieval algorithms. *J. Geophys. Res.* **112**, 1–18.

Weinzierl, B., Petzold, A., Esselborn, M., Wirth, M., Rasp, K. and co-authors. 2008. Airborne measurements of dust layer properties, particle size distribution and mixing state of Saharan dust during SAMUM 2006. *Tellus* **61B**, doi: 10.1111/j.1600-0889.2008.00392.x.

Wu, Z. and Colbeck, I. 1996. Studies of the dynamic shape factor of aerosol agglomerates. *Europhys. Lett.* **33**, 719–724.